RECENT CLEO Υ(1S) and Υ(3S) RESULTS

T.E. COAN
Department of Physics, Southern Methodist University,
Dallas, TX, 75275, USA

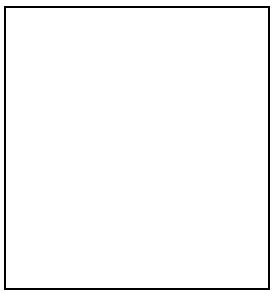

Recent CLEO results on the observation of the $\Upsilon(1D)$ state and a search for the $\eta_b(1S)$ state from a data sample of 4.7×10^6 $\Upsilon(3S)$ decays collected with the CLEO-III detector, and a measurement of the η' production spectrum using 1.9×10^6 $\Upsilon(1S)$ decays collected with the CLEO-II detector are described.

1 Introduction

CLEO is concluding a 1-year program to collect $\sim 4\,\mathrm{fb}^{-1}$ of integrated luminosity distributed over the $\Upsilon(1S), \Upsilon(2S)$ and $\Upsilon(3S)$ resonances. These datasets will augment the world supply of $b\bar{b}$ quark-antiquark bound state data for these resonances by more than an order of magnitude. The data is produced by the symmetric e^+e^- collider CESR and collected by the CLEO-III detector, a configuration of the CLEO detector with excellent electromagnetic calorimetry and enhanced particle identification capabilities.

2 $\Upsilon(1D)$ Observation

Heavy quarkonia (e.g., $b\bar{b}$ quark pairs) are an appealing physical system for probing the strong interactions. Bound states below open flavor threshold are narrow, leading to long lifetimes and little mixing between excitation levels. The constituent quarks are essentially non-relativistic, making the bound state system particularly appropriate for analysis by lattice QCD calculations and by effective theories via potential models.

We present evidence for the observation of the $\Upsilon(1D)$ state, the first observation of a narrow $b\bar{b}$ bound state since the early 1980's, using the following radiative 5-stage cascade decay that ultimately produces 4 photons and a lepton pair in the final state:

$$
\begin{aligned}
\Upsilon(3S) &\rightarrow \gamma\,\chi_b(2P_J) \\
\chi_b(2P_J) &\rightarrow \gamma\,\Upsilon(1D) \\
\Upsilon(1D) &\rightarrow \gamma\,\chi_b(1P_J) \\
\chi_b(1P_J) &\rightarrow \gamma\,\Upsilon(1S) \\
\Upsilon(1S) &\rightarrow e^+e^-, \mu^+\mu^- \qquad (1)
\end{aligned}
$$

The theoretical product branching fraction [1] for this sequential decay is 3.76×10^{-5}. The dominant background reaction is $\Upsilon(3S) \rightarrow \pi^0\pi^0\Upsilon(1S); \Upsilon(1S) \rightarrow e^+e^-, \mu^+\mu^-$. An additional background mode, the same cascade chain as Eq. 1 except that the intermediate $\Upsilon(1D)$ is replaced by the $\Upsilon(2S)$ state, must also be rejected.

Measuring the branching fraction for the background $\Upsilon(3S) \rightarrow \pi^0\pi^0\Upsilon(1S)$ transitions is a useful check of the technique used to reconstruct our cascade signal mode. A key analysis variable $\chi^2_{\pi^0\pi^0}$ used to reconstruct $\Upsilon(3S) \rightarrow \gamma\gamma\gamma\gamma\Upsilon(1S)$ decays is the minimal π^0 mass deviation chi-squared formed from among the three possible photon pairs formed from four individual photons. After cutting on $\chi^2_{\pi^0\pi^0}$, the ratio $\Delta M/\sigma(\Delta M)$ is formed from the deviation of the four-photon recoil mass from the $\Upsilon(1S)$ mass $\Delta M = M_{recoil\,4\gamma} - M_{\Upsilon(1S)}$ and its expected mass resolution $\sigma(\Delta M)$. The distribution $\Delta M/\sigma(\Delta M)$ is shown for data in Fig. 1 fit with a Monte Carlo determined shape. Combining the yield of 737 ± 28 events with a 13.6% Monte Carlo determined efficiency implies a branching fraction $\mathcal{B}(\Upsilon(3S) \rightarrow \pi^0\pi^0\Upsilon(1S)) = (2.33 \pm 0.09 \pm 0.16)\%$, consistent with, but more precise than, previous measurements [2,3].

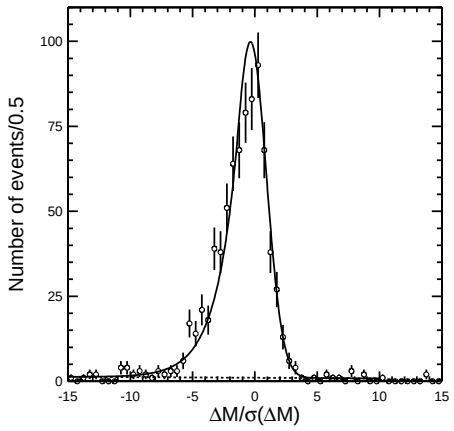

Figure 1: Distribution of the recoil mass deviation from the $\Upsilon(3S)$ mass for $\Upsilon(3S) \rightarrow \pi^0\pi^0\Upsilon(1S)$ candidate events. Dots are data, solid line is fit.

Confident that our technique for reconstructing multiple photons in a single event is robust, we select $\Upsilon(1D)$ events by constructing a chi-squared based variable $\chi^2(1D)$ that is a function of the unknown $\Upsilon(1D)$ mass and the total angular momentum J of the χ_b states on either side of the $\Upsilon(1D)$ in the cascade chain. Other chi-squared based variables are used to reject background. Surviving events are shown in the left hand side of Fig 2 as the histogram with the signal region $\chi^2(1D) \leq 10$. The fit of the signal on top of the background is shown as the heavy and dashed lines, respectively, producing a significance of 9.7σ.

The $\Upsilon(1D)$ mass is estimated by plotting for each event in the signal region of the left hand plot in Fig. 2 the value of the mass that minimizes $\chi^2(1D)$. Monte Carlo studies predict a peak at the true mass plus two satellite peaks due to mis-reconstructed photons from shower

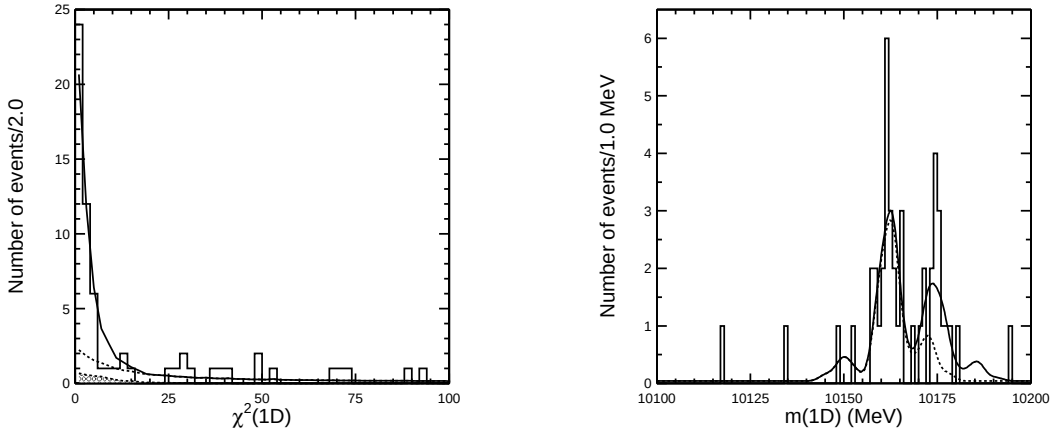

Figure 2: The left hand side is a fit to the χ^2_{1D} for data. The solid line is a fit to the signal contribution on top of backgrounds. The right hand side is a fit of a two-peak structure to the most-likely mass taken from the signal region of the left hand plot.

leakage in the calorimeter. The mass distribution for data is shown as the histogram in the right hand plot of Fig. 2. Although the $\Upsilon(1D)$ can be produced in any of the $J = 1, 2, 3$ states, our selection efficiency is largest for the $\Upsilon(1D_1)$ and $\Upsilon(1D_2)$ states while theory predicts that the $\Upsilon(1D_2)$ state should be preferentially produced in the decay cascade. Fitting the histogram with two peaks, each with two satellites, produces a peak at $M_{low} = 10161.2 \pm 0.7\,\mathrm{MeV/c^2}$ and at $M_{high} = 10174.2 \pm 1.3\,\mathrm{MeV/c^2}$, with an overall 58% C.L. Fitting under the assumption that there is no low mass peak produces a 0.04% C.L. and the difference in significance between these two fits implies a significance of the low mass peak of 6.8σ. Fitting the histogram with just a single peak plus two satellites yields a 43% C.L. fit with a peak at $10162.0 \pm 0.5\,\mathrm{MeV/c^2}$.

Averaging over the different fits yields a $\Upsilon(1D)$ mass of $10162.2 \pm 1.6\,\mathrm{MeV/c^2}$ with the $J = 2$ state favored, but the $J = 1$ state not excluded. Based on our measured $\Upsilon(1D)$ yields and Monte Carlo determined efficiency, the preliminary overall branching fraction for the 5-stage decay cascade of the $\Upsilon(3S)$ via the $\Upsilon(1D)$ is $(3.3 \pm 0.6 \pm 0.5) \times 10^{-5}$.

3 Search for $\eta_b(1S)$

The spin-singlet state of the $b\bar{b}$ system, including the $b\bar{b}$ ground state $\eta_b(1S)$, has yet to be observed. The reaction $e^+e^- \to \gamma^* \to b\bar{b}$ produces $b\bar{b}$ states with the same J^{PC} quantum numbers as the photon so the $\eta_b(1^1S_0)$ state cannot be produced directly at CESR. However, the state is accessible through decays from the spin-triplet $\Upsilon(nS)$ states via magnetic dipole (M1) radiative transitions which occur between states with opposite quark spin configuration but the same orbital angular momentum. The rate for M1 transitions between the Υ and the η_b is given by [4]

$$\Gamma[\Upsilon(nS) \to \gamma\,\eta_b(n'S)] \propto I^2 E_\gamma^3, \tag{2}$$

where n and n' are the principal quantum numbers of the respective $b\bar{b}$ systems, I is an overlap integral between initial and final $b\bar{b}$ states and E_γ is the energy of the emitted photon.

With a data sample of 4.7×10^6 $\Upsilon(3S)$ events, CLEO searches for transitions with $n \neq n'$ to avoid photon energies in the 100 MeV range which are susceptible to background contamination from π^0 decays. The inclusive photon search technique for $\Upsilon(3S) \to \gamma\eta_b(1S)$ is tuned using the

electric dipole (E1) transitions $\chi_b(2P) \to \Upsilon(1S)$ where the photon energy is $\sim 800\,\mathrm{MeV}$, similar to what is expected [4] for the signal M1 transition.

The inclusive photon spectrum between approximately 550 MeV and 1 GeV is shown in the left hand side of Fig. 3 where the dots indicate data and the dashed line is background. A logarithmic energy scale is used to preserve energy resolution. The central peak is a superposition of three gaussians for the three $\chi_b(2P_J)$ E1 transitions and the search window is also indicated.

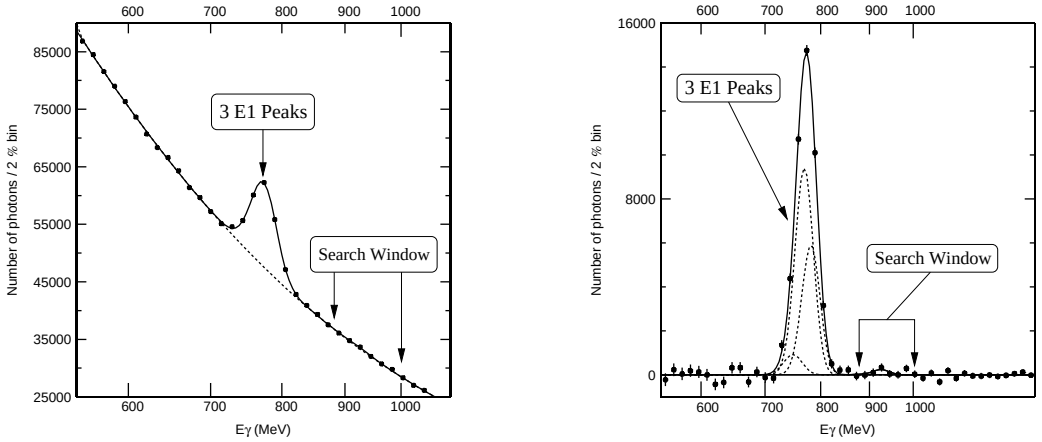

Figure 3: The inclusive photon spectrum in the E1 peak and the η_b search region before (left) and after (right) background subtraction.

The right hand side of Fig. 3 shows the background subtracted central peak and the search region fitted with a Crystal Ball lineshape. Multiple fits are performed for various photon energies in the search region and no signal is seen. This lack of signal is converted into a 90% C.L. upper limit shown in Fig. 4, excluding a variety of phenomenological models [4].

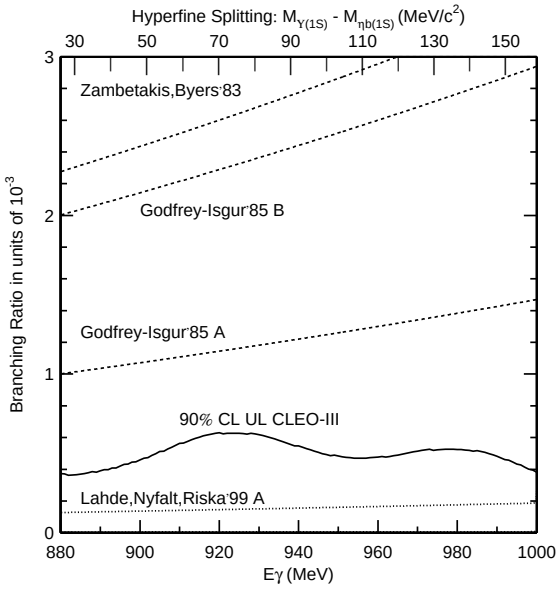

Figure 4: Upper limits on $\mathcal{B}(\Upsilon(3S) \to \gamma\,\eta_b(1S))$ as a function of E_γ. Model predictions are from Ref. [4].

4 $\Upsilon(1S) \to \eta' X$ Production

An unexpectedly large $B \to \eta' X_s$ inclusive decay rate in the momentum range $2 \leq p_{\eta'} \leq 2.7$ GeV/c observed by CLEO[5] and BABAR[6] is possibly described by an anomalously large coupling between the η' and two gluons[7,8,9] in the underlying $b \to sg$ mechanism thought responsible for η' production. Here the process $b \to sg$ is followed by the two gluon coupling to the η' shown in Fig. 5.

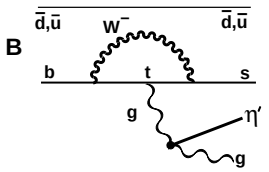

Figure 5: Feynman diagram for $b \to sg\eta'$.

The effective $\eta' g^* g$ coupling can be written as[10]

$$H(q^2)\epsilon_{\alpha\beta\mu\nu} q^\alpha k^\beta \epsilon_1^\mu \epsilon_2^\nu, \tag{3}$$

where $H(q^2)$ is the $\eta' g^* g$ transition form factor, $q = p_b - p_s$ is the four-momentum of the virtual hard gluon (g^*) and k is the momentum of the soft gluon (g). Workers[10] have shown that the q^2 region relevant to the process $b \to sg\eta'$ is accessible in high energy η' production in $\Upsilon(1S)$ decays so that constraints can be placed on $H(q^2)$ from the fast η' spectrum in $\Upsilon(1S) \to ggg$ decays. Various choices[8,10] are available for $H(q^2)$.

We use 1.86×10^6 $\Upsilon(1S)$ decays collected with the old CLEO II detector and detect η' mesons through the decay channel $\eta' \to \eta\pi^+\pi^-(\eta \to \gamma\gamma)$. This data sample can be divided into three parts:

$$N_{all} = N_{\Upsilon(1S)\to ggg} + N_{\Upsilon(1S)\to q\bar{q}} + N_{e^+e^-\to q\bar{q}}\,, \tag{4}$$

where the last piece is the most problematic background to correct for. We do this by using 1.19 fb^{-1} of off-resonance data collected just below the $\Upsilon(4S)$ resonance by a process that maps the η' production spectra at the higher $\Upsilon(4S)$ energy to the lower $\Upsilon(1S)$ energy by a procedure analogous to what is done when one maps one normalized probability distribution into another one with a different domain. The remapping is done with the aid of the variable $Z = E_{\eta'}/E_{beam}$, the fractional energy of the η'.

Defining three differential branching fractions dn/dZ

$$\begin{aligned}
\frac{dn(ggg)}{dZ} &= \frac{d\mathcal{B}(\Upsilon(1S) \to ggg \to \eta' X)}{dZ \times \mathcal{B}(\Upsilon(1S) \to ggg)} \\
\frac{dn(q\bar{q})}{dZ} &= \frac{d\mathcal{B}(\Upsilon(1S) \to q\bar{q} \to \eta' X)}{dZ \times \mathcal{B}(\Upsilon(1S) \to q\bar{q})} \\
\frac{dn(1S)}{dZ} &= \frac{d\mathcal{B}(\Upsilon(1S) \to \eta' X)}{dZ}
\end{aligned}$$

permits us to use the Z spectrum of η' and discriminate among the various phenomenological models that predict different forms of $H(q^2)$. Fig. 6 shows the comparison between the measured $dn(ggg)/dZ$ spectrum (dots) and various phenomenological predictions (histograms). Only the region $Z \geq 0.7$ is relevant for comparison since the models require the η' be "fast." The model labeled "b" is representative of perturbative QCD [11,12] and fits the data best. There is no evidence for any anomalously high $\eta' g^* g$ coupling at large η' energies.

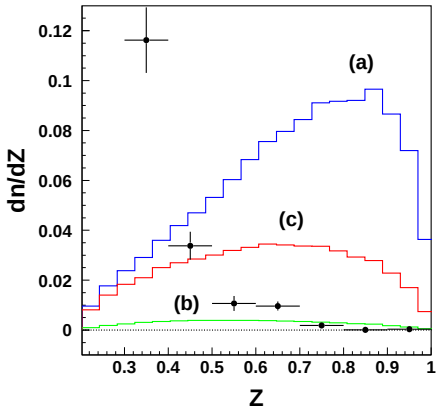

Figure 6: Measured dn/dZ spectrum of $\Upsilon(1S) \to ggg \to \eta' X$ compared with theoretical predictions. See text for explanation.

Acknowledgments

The author acknowledges support by the U.S. Department of Energy under grant DE-FG03-95ER40908.

References

1. S. Godfrey and J.L. Rosner, PRD **64**, 097501 (2001); W. Kwong and J.L. Rosner, PRD **38**, 279 (1988).
2. F. Butler *et al.*, (CLEO II), PRD **49**, 40 (1994).
3. U. Heintz *et al.*, (CUSB), PRD **46**, 1928 (1992).
4. S. Godfrey and J.L. Rosner, PRD **64**, 074011 (2001).
5. T.E. Browder *et al.*, PRL **81**, 1786 (1998).
6. B. Aubert *et al.*, hep-ex/0109034.
7. D. Atwood and A. Soni, PLB **405**, 150 (1977).
8. W.S. Hou and B. Tseng, PRL **80**, 434 (1998).
9. A.L. Kagan and A.A. Petrov, hep-ph/9707354.
10. A.L. Kagan, hep-ph/0201313.
11. A. Ali and A.Y. Parkhomenko, PRD **65**, 074020 (2002).
12. T. Muta and M.-Z. Yang, PRD **61**, 054007 (2000).